THE JOURNAL OF BIOLOGICAL CHEMISTRY
Vol. 278, No. 50, Issue of December 12, pp. 50163–50174, 2003
Printed in U.S.A.

Cell Swelling Stimulates Cytosol to Membrane Transposition of ICln*

Received for publication, January 13, 2003, and in revised form, September 8, 2003
Published, JBC Papers in Press, September 11, 2003, DOI 10.1074/jbc.M300374200

Markus Ritter‡§, Andrea Ravasio‡, Martin Jakab‡, Sabine Chwatal‡, Johannes Fürst‡, Andreas Laich‡, Martin Gschwentner‡, Sara Signorelli‡, Carmen Burtscher‡, Sonja Eichmüller‡, and Markus Paulmichl‡¶‖

From the ‡Department of Physiology, University of Innsbruck, Fritz-Pregl-Strasse 3, A-6020 Innsbruck, Austria and the ¶Department of Biomolecular Science and Biotechnology, Università degli Studi di Milano, Via Celoria 26, I-20133 Milan, Italy

ICln is a multifunctional protein that is essential for cell volume regulation. It can be found in the cytosol and is associated with the cell membrane. Besides its role in the splicing process, ICln is critically involved in the generation of ion currents activated during regulatory volume decrease after cell swelling (RVDC). If reconstituted in artificial bilayers, ICln can form ion channels with biophysical properties related to RVDC. We investigated (i) the cytosol *versus* cell membrane distribution of ICln in rat kidney tubules, NIH 3T3 fibroblasts, Madin-Darby canine kidney (MDCK) cells, and LLC-PK$_1$ epithelial cells, (ii) fluorescence resonance energy transfer (FRET) in living fibroblasts between fluorescently tagged ICln and fluorochromes in the cell membrane, and (iii) possible functional consequences of an enhanced ICln presence at the cell membrane. We demonstrate that ICln distribution in rat kidneys depends on the parenchymal localization and functional state of the tubules and that cell swelling causes ICln redistribution from the cytosol to the cell membrane in NIH 3T3 fibroblasts and LLC-PK$_1$ cells. The addition of purified ICln protein to the extracellular solution or overexpression of farnesylated ICln leads to an increased anion permeability in NIH 3T3 fibroblasts. The swelling-induced redistribution of ICln correlates to altered kinetics of RVDC in NIH 3T3 fibroblasts, LLC-PK$_1$ cells, and MDCK cells. In these cells, RVDC develops more rapidly, and in MDCK cells the rate of swelling-induced depolarization is accelerated if cells are swollen for a second time. This coincides with an enhanced ICln association with the cell membrane.

The ability of volume regulation is a fundamental feature of cells. On the one hand, cells are persistently challenged by disturbances of the osmotic equilibrium between intra- and extracellular space due to changes in the ambient osmolarity, metabolism of osmotically active solutes or ion- and substrate transport. On the other hand, cells have to change their volume to execute specific functions such as cell division, migration, or secretion. Accordingly, cell volume regulatory mechanisms are involved in various cell functions, and disturbances of these mechanisms can lead to severe dysfunctions (1, 2).

The *ad hoc* mechanism that enables cells to down-regulate their volume after swelling, a process called regulatory volume decrease (RVD),[1] is realized by the export of cellular ions and osmotically obliged water by the activation of ion channels. Besides K^+ channels, most cells activate a distinct class of anion channels (termed IClvol, IClswell, volume-regulated anion channel, or volume-sensitive osmolyte and anion channel). Interestingly, these channels are also permeable to cations, organic osmolytes, and possibly ATP. Therefore, the (an)ion channels and the respective currents that are activated by cell swelling have recently been termed and are here referred to as regulatory volume decrease channels/currents (RVDC) (3, 4).

The phenotypes of RVDC vary between cells but display some fingerprint features: they can be blocked by chloride channel blockers and extracellular nucleotides, are outwardly rectifying, inactivate at positive potentials, and are permeable to organic osmolytes and to both anions and cations in a manner depending on pH, calcium concentration, and lipid composition (3). The molecular identity of RVDC is still elusive if we expect a one-molecule/one-function relation, *i.e.* that one molecule is responsible for generating all of the heterogeneous current phenotypes observed after cell swelling in different cells. However, several candidate-proteins can be envisioned to be involved in the formation of functional RVDC, such as ATP binding cassette transporters (P-glycoprotein, MDR1, CFTR), phospholemman, voltage-dependent anion channels, the CLC family of chloride channels (CLC2 and CLC3), and ICln (3).

ICln is a highly conserved and ubiquitously expressed protein that has been identified in all cells studied so far. The human gene for ICln is located on chromosome 11q13.5–14.1

* This article was supported in part by the Austrian Science Foundation (FWF, Grants P12337, P13041, P12467, and P14102Med), the Austrian National Bank (Grants 8444 and 6994), and the Gastein Foundation (Grant FP41/FP46) (to M. P. and M. R.). The costs of publication of this article were defrayed in part by the payment of page charges. This article must therefore be hereby marked "*advertisement*" in accordance with 18 U.S.C. Section 1734 solely to indicate this fact.

§ To whom correspondence may be addressed. Tel.: 43-512-507-3766; Fax: 43-512-507-2853; E-mail: markus.ritter@uibk.ac.at.

‖ To whom correspondence may be addressed. Tel.: 43-512-507-3756; Fax: 43-512-577-656; E-mail: markus.paulmichl@uibk.ac.at.

[1] The abbreviations used are: RVD, regulatory volume decrease; RVDC, regulatory volume decrease currents/channels; CLIC, chloride intracellular channel; ECFP, enhanced cyan fluorescent protein; EYFP, enhanced yellow fluorescent protein; FRET, fluorescence resonance energy transfer; ICln, I = current, Cl = chloride, and n = nucleotide-sensitive; ICln-CAAX, farnesylation sequence (K-ras-derived CAAX-motive, MSKDVKKKKKKSKTKCVIM) attached to ICln; IClswell, swelling-dependent chloride current; IClvol, volume-dependent chloride current; IGSS, immunogold silver staining; MDCK cells, Madin-Darby canine kidney cells; MEQ, 6-methoxy-*N*-ethyl-1,2-dihydroquinoline; 2-ME, 2-mercaptoethanol; ORF, open reading frame; PBS, phosphate-buffered saline; PD, cell membrane potential; QR, quenching rate; ROI, region of interest; TBS, Tris-buffered saline; CFP-ICln, fusion protein of ICln attached to the C terminus of ECFP; CFP-Mem, palmitoylation sequence (N-terminal 20 amino acids of neuromodulin/GAP-43) attached to ECFP; YFP-ICln, fusion protein of ICln attached to the C terminus of EYFP; YFP-Mem, palmitoylation sequence attached to EYFP.

and controlled by a constitutively highly active promoter (5). The protein is essential for life, because all attempts to genetically knock out ICln in either mice, nematodes, or a cell line failed due to the lethality of the knockout (6).[2] ICln is mainly found to be a water-soluble protein in the cytosol, but some portion is found within or in close association with the cell membrane. Different functions have been discussed for ICln. Overexpression of ICln in *Xenopus laevis* oocytes results in the occurrence of ion currents with features closely resembling RVDC. Accordingly it was assumed that ICln could form the ion conductive part of RVDC (7). A knockdown of the ICln protein with ICln-specific antibodies (8) or antisense oligodeoxynucleotides (9–11) leads to a significant reduction of RVDC in native cells, whereas overexpression of ICln increases RVDC amplitudes and accelerates the activation of RVDC during a hypotonic challenge (11). Overexpression of ICln or ICln related peptides in *Escherichia coli* renders the bacteria tolerant to hypotonicity, an effect that can be reversed by extracellular nucleotides (12, 13). Reconstitution of purified ICln in lipid bilayers indeed revealed that the protein can form ion channels and the induced current displays fingerprint features of RVDC. ICln reconstituted in heart lipid is anion selective, in artificial lipids it is cation selective, with relative permeability sequences matching those of RVDC (14–17).

Analysis of the amino acid sequence of ICln predicts a transmembrane domain in the N-terminal half of the protein. This sequence shows a remarkable similarity to the pore-forming β-hairpin of α-hemolysin and leukocidin, which are water-soluble bacterial toxins that refold and build large pores upon insertion into cell membranes. Secondary structure and hydrophobicity pattern prediction suggests a transmembrane domain that is composed of a four-stranded β-sheet. To form a functional channel, the formation of an ICln dimer is required. The model of the ICln channel has been refined by site-directed mutagenesis experiments (7, 14, 16, 18).

All of these findings clearly link ICln functionally to RVD. It is however still a matter of debate, as to whether the protein itself is a part of the molecular RVDC complex or rather acts as a regulator thereof (4, 14), *e.g.* by interacting with integral membrane proteins or membrane-associated molecules. In addition to its role in volume regulation, ICln has recently been shown to interact with methylosomes, a cytoplasmatic complex involved in RNA splicing (19–22), suggesting a multifunctional role for this protein.

An intriguing feature of ICln is that it can appear in a water-soluble form, as well as in close association with the cell membrane. The mechanisms by which soluble ICln protein associates with and/or incorporates itself into the membrane are unknown. The present study has been performed to further investigate the intracellular distribution of ICln under normal conditions and during hypo-osmotic stress, as well as to correlate an enhanced presence of membrane-bound ICln with functional changes of the cell.

EXPERIMENTAL PROCEDURES

Salts, Chemicals, Drugs, and Optical Filters

All salts, chemicals, and drugs were of *pro analysi* grade and purchased from Sigma, Germany unless otherwise stated. Cell culture reagents were from Invitrogen, Germany. Optical filters were purchased from AHF Analysentechnik, Germany.

Plasmids and Fusion Proteins

Standard procedures (23) and procedures according to the manufacturers' protocols were used for DNA preparation, cloning, purification, and sequencing. Plasmids coding for fusion proteins of ICln attached to the C terminus of ECFP or EYFP (CFP-ICln and YFP-ICln) were prepared by cloning the ORF coding for the canine (MDCK) ICln in-frame into the vectors pECFP-C1 and pEYFP-C1 (Clontech) using the XhoI and BamH1 restriction sites. For cell membrane labeling with fluorescent proteins (CFP-Mem and YFP-Mem) the vectors pECFPMem and pEYFPMem (Clontech) were used. To enhance targeting of ICln to the cell membrane, cells were transfected with the pCDNA3YFPCaaX vector (24, 25), in which YFP was replaced by ICln (ICln-CAAX). The same vector lacking the ICln and YFP insert was used as a control vector. All constructs were sequenced using an automated sequencer (Gene ReadIR 4200, LiCor).

Protein Purification

The ORF of ICln was cloned in-frame into the pET3-His vector, which adds a histidine tag to the N terminus of ICln (14). The protein was expressed in *E. coli* (BL21/DE3), purified using a nickel-nitrilotriacetic acid-agarose column (Qiagen) and stored at −74 °C in 50 mM K_2HPO_4, 200 mM imidazole, pH 8.00.

Cell Culture and Transfections

NIH 3T3 fibroblasts, LLC-PK_1 cells, and MDCK cells (strain II, low resistance) were grown in culture dishes in Dulbecco's modified Eagle's medium supplemented with 10% fetal calf serum, 100 μg/ml penicillin, and 100 units/ml streptomycin, at 37 °C and 5% CO_2 and 95% air. Subcultures were routinely established every second to third day by trypsin/EDTA treatment (0.05%, pH 7.2). Cells were used for experiments at a degree of confluency of ~40–70% unless otherwise stated.

For transfection with the appropriate plasmids, NIH 3T3 fibroblasts were grown to 70% confluency and incubated for 6 h with 3 μg of plasmid DNA and 7 μl of LipofectAMINE 2000™ (Invitrogen). For double transfection with CFP-ICln and YFP-Mem a ratio of 2:1 yielded the best results. Thereafter the cells were subcultured and grown on uncoated glass cover slips for 24–48 h. The transfection efficacy was ~15–20%.

Fluorescence Resonance Energy Transfer Measurements

For all FRET experiments, ECFP served as a donor and EYFP as an acceptor (26–29). Cells were cotransfected with CFP-ICln and YFP-Mem (schematically shown in Fig. 1*A*) or with CFP-Mem and YFP-ICln. Transfected cells were superfused at room temperature (20–23 °C) with a control solution (in mM: NaCl 90, KCl 5, $CaCl_2$ 2, $MgCl_2$ 2, glucose 5, mannitol 80, HEPES 10, pH 7.4) or hypotonic solution (omission of mannitol). Visualization of ECFP- and/or EYFP-expressing cells and detection of FRET was performed on an Olympus IX70 inverted microscope equipped with a monochromator (Polychrome 4, TILL Photonics) and a cooled charge-coupled device camera (TILL Imago SVGA) controlled by the TILL Vision software (versions 3.3 and 4.0). Experiments were either performed by changing three separate Olympus BX cubes equipped with the appropriate filter combinations for ECFP, EYFP, and FRET measurements or by using a CFP/YFP dual-band polychroic mirror in combination with a real-time dual color imaging device (DualView™, Optical Insights) (Table I). All images were adjusted to pixel-by-pixel alignment and corrected for background, which was then clamped to zero (29).

Acceptor Photobleaching

Light from a xenon lamp (XBO 75, Osram) was passed through a 515-nm cutoff filter toward the object. The FRET efficiency ($FRET_{eff}$) was calculated from the increase in ECFP intensity after the bleaching of EYFP: $FRET_{eff} = 1 - (I_{CFP\text{-}bg}DA/I_{CFP\text{-}bg}D)$, where $I_{CFP\text{-}bg}DA$ and $I_{CFP\text{-}bg}D$ are the background-corrected fluorescence intensities of ECFP in the presence of both donor and acceptor and in the presence of the donor alone, respectively. As shown in Fig. 1 (*B* and *C*) YFP-Mem is bleached to 11 ± 2% ($n = 6$) within 10 min. This is paralleled by an increase of the CFP-ICln fluorescence to 114 ± 5% ($n = 6$). The calculated FRET efficiency after 10 min is 0.11 ± 0.04 ($n = 6$) and 0.20 ± 0.03 ($n = 6$) if calculated from the entire area of the cell and from selected regions close to the cells' outer margins, respectively. Fig. 1*D* shows the calculated FRET efficiency image of the cells shown in Fig. 1*C*.

NFRET Calculation

Corrected FRET images (NFRET) were calculated from the sensitized emission of EYFP (29). Each of the images was corrected for ECFP cross-talk (*i.e.* contribution of ECFP emission to the EYFP emission window) and EYFP cross-excitation (*i.e.* EYFP emission due to excitation at 436 nm), and this is referred to as,

[2] M. Ritter, A. Ravasio, M. Jakab, S. Chwatal, J. Fürst, A. Laich, M. Gschwentner, S. Signorelli, C. Burtscher, S. Eichmüller, and M. Paulmichl, unpublished observations.

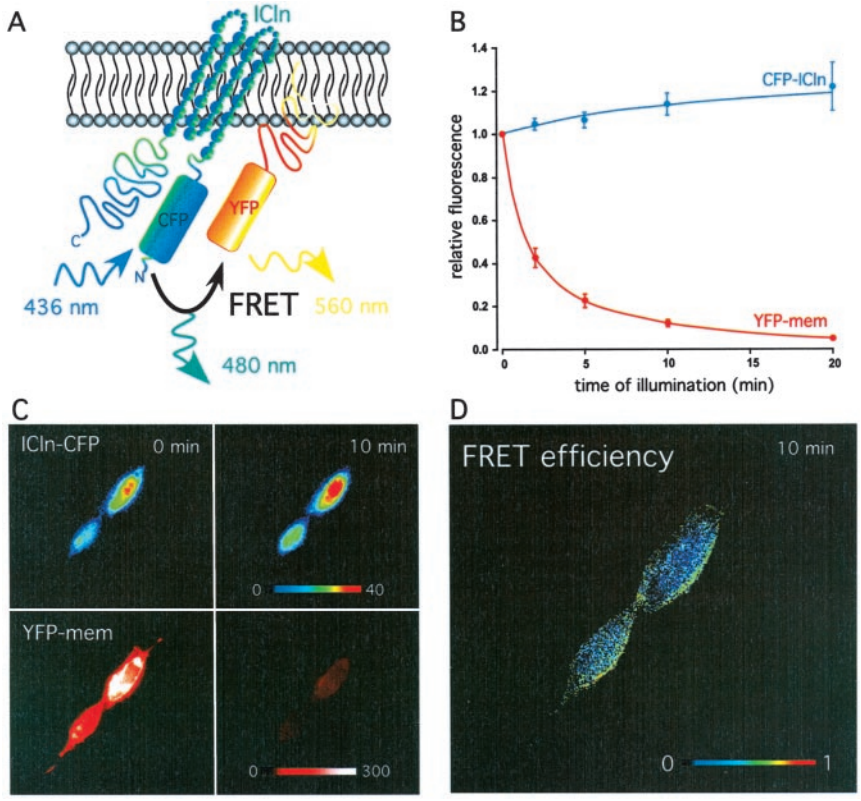

FIG. 1. *A*, model of FRET between a CFP-ICln fusion protein (acting as a donor) and a palmitoylated/farnesylated EYFP protein (YFP-Mem; acting as an acceptor). ECFP is fused to the N terminus of ICln, which is depicted according to the proposed channel model (7). EYFP is attached to the cell membrane by its lipid anchor, and FRET can only occur if the two proteins are within a distance of ~10–90 Å, *i.e.* if CFP-ICln is inserted or attached to the cell membrane. Upon FRET, the donor emission at 480 nm decreases and the acceptor emission at 560 nm increases. *B–D*, acceptor photobleaching experiments. Cells cotransfected with CFP-ICln and YFP-Mem were illuminated for 20 min with light of a wavelength of >515 nm, thus bleaching YFP-Mem. The parallel increase in the fluorescence of CFP-ICln unmasks the energy transfer. *B*, time courses of the relative changes of the fluorescence intensities for CFP-ICln and YFP-Mem during photobleaching (means ± S.E.). *C*, representative image of cells during photobleaching. *D*, calculated image of the FRET efficiency. Note that the regions in the outer perimeter of the cell exhibit the most intense FRET efficiency.

TABLE I
Filters used for FRET experiments

All filters were purchased from AHF Analysentechnik, Germany.

	Excitation	Excitation filter	Beamsplitter 1	Beamsplitter 2	Emission filter
	nm				
Single-cube setup					
ECFP	436	436/20	455 DCLP		480/40
EYFP	515	510/20	530 DCLP	560/40	
FRET	436	436/20	455 DCLP	560/40	
Dual-View™ setup					
ECFP	436		CFP/YFP-dual-band[a]	505 DCLP	480/40
EYFP	515		CFP/YFP-dual-band[a]	505 DCLP	560/40
FRET	436		CFP/YFP-dual-band[a]	505 DCLP	560/40
Acceptor photobleaching					
EYFP	>515	515 LP			

[a] Part no. F86-004.

netFRET = $I_{\text{FRET-bg}} - (I_{\text{CFP-bg}} \times k_1) - (I_{\text{YFP-bg}} \times k_2)$, where $I_{\text{FRET-bg}}$, $I_{\text{CFP-bg}}$, and $I_{\text{YFP-bg}}$ are the background-corrected pixel gray values in the windows for FRET (ex, 436; em, 560 nm), ECFP (ex, 436; em, 480 nm), and EYFP (ex, 515; em, 560 nm), and k_1 and k_2 denote the relative contribution to the fluorescence intensity in the FRET window by ECFP cross-talk (k_1) and EYFP cross-excitation (k_2). For the excitation wavelengths and filter combinations provided in Table I, k_1 and k_2 were measured to be 0.3 and 0.04, respectively. These values did not change significantly under hypotonic conditions. The obtained netFRET values were normalized against protein expression levels and are referred to as, NFRET = netFRET × $100/(I_{\text{CFP-bg}} \times I_{\text{YFP-bg}})^{1/2}$ (29). The integrated fluorescence density values of the images from total cells or from particular regions of interest therein were analyzed using TILL Vision and Microsoft Excel software.

Because the fluorescence of green fluorescent protein and its variants is sensitive to pH (30), FRET could be affected by swelling-induced intracellular acidification (31). During cell swelling the relative fluorescence of YFP-Mem decreased by 5.5 ± 2.3% (n = 17), and the measured FRET signals are therefore likely to be underestimated.

Immunohistochemistry/Immunogold Silver Staining (IGSS)

Rat kidneys were removed after sacrifice, decapsulated, and cut into 2-mm sections from which the cortex, outer medulla, inner medulla, and papilla regions were separated (Fig. 2), washed in ice-cold PBS (pH 7.4), frozen and stored at −70 °C until further processing for Western analysis. For IGSS, the sections were fixed overnight (2.5% glutaraldehyde in PBS), washed in PBS, dehydrated in ethanol, incubated in xylol and paraplast, cut to 6-μm sections, and placed on poly-L-lysine-coated glass coverslips. Thereafter the paraplast was removed, the specimens were rehydrated, rinsed in distilled water and PBS (32), incubated in diluted (1:10) normal rabbit serum, then placed for 1 h in the primary polyclonal rabbit anti-ICln-antibody-containing solution (14), washed and incubated with the labeled (10-nm gold) secondary anti-rabbit IgG antibody. Then the samples were extensively washed, incubated in the dark for 5–10 min in a 1:1 mixture of hydrochinon and silver acetate (British Bio Cell International), washed extensively again in distilled water, subjected to iron hematoxilin staining and evaluated on a confocal laser-scanning microscope (LSM 410, Zeiss). The images obtained from the light reflections from the silver grains were overlaid with the conventional confocal transmission images.

SDS-PAGE and Western Analysis

Subconfluent NIH 3T3 fibroblasts, LLC-PK_1 cells, MDCK cells, or confluent LLC-PK_1 cells were washed with PBS, detached by gentle treatment with trypsin, suspended in isotonic PBS, centrifuged for 10 min (700 × g, room temperature) and resuspended for 15 min in either isotonic or hypotonic buffer at 37 °C. The buffers were composed of (mM): phenylmethylsulfonyl fluoride 0.1, 2-ME 5 in PBS (pH 7.4; 310 mosM) and phenylmethylsulfonyl fluoride 0.1, 2-ME 5, Tris-HCl 20, in distilled water (pH 7.4; 110 mosM). Thereafter, the cells were homoge-

nized by repeated freeze-thawing cycles (liquid nitrogen/37 °C) or by sonication (5–20 s, 4 °C) in lysis buffer (33). The cell lysates were centrifuged for 1 h at 100,000 × *g* at 4 °C. Supernatant (cytosolic fraction) and pellet (membrane fraction) were separated, and 2 μl of each supernatant was used to determine the protein concentration (34). Sample buffer (4× SDS-PAGE) was added to each sample containing supernatant. A volume of 1× SDS-PAGE sample buffer, equal to the volume of the corresponding supernatant sample, was added to the respective membrane fraction. Samples were then vortexed, heated to 100 °C for 5 min, centrifuged (19,000 × *g*, 5 min), and separated on a 13% SDS-PAGE according to the method of Laemmli (35). A volume containing 100 μg of cytosolic protein, and an equal volume from the corresponding membrane-sample was loaded onto the gel for electrophoretic protein separation. Thus the same relative amounts of the total cytosolic proteins and total membrane proteins, respectively, of a given cell preparation were separated. Proteins were then electroblotted (23) onto a nitrocellulose membrane (Amersham Biosciences). Membranes were blocked in TBS containing 1% Tween and 5% nonfat dry milk for 1 h at room temperature, followed by incubation with primary anti-ICln polyclonal antibody for 1 h, washing, incubation with secondary antibody (1:2500) in TBST and antibody detection by enhanced chemiluminescence (ECL™-System, Amersham Biosciences). Significant immunoreactivity was detected only at an apparent molecular mass of 36 kDa. Densitometric quantification was performed for the 36-kDa bands (ImageQuant™, Amersham Biosciences or Eagle Eye™, Stratagene). Data from subconfluent and confluent LLC-PK_1 cells were pooled.

Electrophysiology

Whole Cell Patch Clamp and Perforated Patch Clamp Measurements—Cells were used 24–48 h after splitting. All experiments were performed at room temperature. For data acquisition and analysis, an EPC-9 (HEKA) or Axopatch 200A (Axon Instruments) amplifier, as well as Pulse/Pulsefit software (HEKA) were used. Current signals were filtered at 1 kHz (4-pole Bessel). The holding potential was 0 mV. The time courses of current activation were monitored by applying pulses (0.5 s) to +40 mV at intervals of 10 s. Current-voltage relations were registered by pulsing (0.5 s) from −120 mV to +100 mV with step increments of 20 mV or by applying a voltage ramp (−120 mV to +100 mV, 0.5 s). Bath and pipette solutions were composed for measuring swelling-activated chloride currents. The extracellular control solution was (mM): NaCl 125, $MgCl_2$ 2.5, $CaCl_2$ 2.5, HEPES 10, mannitol 50, pH 7.2. Because cells usually display slight swelling under isotonic conditions upon establishment of the whole cell configuration, the osmolarity of the extracellular control solution was increased to 375 mosM by mannitol. The pipette solution was (mM): CsCl 125, $MgCl_2$ 5, EGTA 11, MgATP 2, raffinose 50, pH 7.2 (adjusted with CsOH), 340 mosM. RVDC was monitored while cells were kept for 1.5 min under control conditions, followed by two successive pulses of hypotonicity (omission of mannitol; duration, 3 min for NIH 3T3 fibroblasts, 5 min for LLC-PK_1 cells and MDCK cells), which were separated by a 3- to 5-min lasting control period (approach 1).

During prolonged experiments in the whole cell configuration, intracellular compounds might be diluted or dialyzed out of the cell. To exclude that this accounts for some of the observed effects, additional sets of experiments were performed. NIH 3T3 fibroblasts were kept in the on-cell configuration under control conditions for 1.5 min. Cells were then either exposed to hypotonicity for 3 min or kept under control conditions for the same period. Then the whole cell configuration was established, and cells were kept under control conditions for 3 min, followed by a 3-min period of hypotonicity (approach 2). To determine reversal potentials of RVDC, 125 mM NaCl were replaced by 125 mM CsCl in the hypotonic solution, which was subsequently exchanged for a solution containing 12.5 mM CsCl and 255 mM mannitol. The bath was connected to the reference AgCl electrode via a 3 M KCl agar bridge. In a separate set of experiments we used the perforated patch clamp method with nystatin. The tips of the recording electrodes were dipped into a nystatin-free pipette solution for 2–3 s and then backfilled with pipette solution containing nystatin (120 μg/ml). Gigaseals were formed 30–45 s after pipette filling. Current recordings were started after the access resistance decreased to 10–15 MΩ (approach 3).

Cell Membrane Potential Measurements—PD was measured in subconfluent MDCK cells using conventional microelectrodes as described earlier (31). The extracellular superfusate was composed of (mM): NaCl 81 or 41, KCl 5.4, $MgCl_2$ 0.8, $CaCl_2$ 1.2, Na_2HPO_4 0.8, NaH_2PO_4 0.2, $NaHCO_3$ 20, glucose 5.5, and mannitol 70 or 150. The solutions were equilibrated with 5% CO_2 and 95% air (pH 7.4) and a temperature of 37 °C. Hypotonicity was established by the omission of mannitol.

MEQ Fluorescence Quenching

diH-MEQ (Molecular Probes) was prepared as described earlier (36). Cells were loaded for 10 min with 5 μM diH-MEQ, washed, and superfused with either a control solution (in mM: sodium gluconate 131, potassium gluconate 5.4, $MgSO_4$ 0.8, calcium gluconate 1.2, NaH_2PO_4 1, glucose 5.5, Tris 5, pH 7.4), or with a hypotonic solution (sodium gluconate reduced to 81 mM). The solution was then exchanged rapidly for a 150 mM KSCN solution, and the decrease of the MEQ fluorescence due to cellular anion entry was taken as a measure for the anion permeability of the cell membrane (36). Measurements were performed on an Olympus IX70 microscope equipped with a monochromator (SpectraMaster, LSR) and a cooled charge-coupled device camera (Olympix FKI 300) controlled by the Merlin™ software (LSR). Cells were excited at 340 nm. Emitted light was directed through a 420-nm cutoff filter. The images were background corrected and analyzed using Esprit™ Software (LSR) and Microsoft Excel.

Animal Procedures

Male Munich Wistar rats (415–425 g, Ivanovas, Germany) were anesthetized by ether narcosis and subsequent intraperitoneal injection of Trapanal (100 mg/kg body weight). A catheter was placed in the right jugular vein and isotonic saline (145 mM NaCl, 5 mM KCl) was infused at a rate of 62 μl/min. Furosemide was administrated at a concentration of 42 μg/ml for 1 h and of 420 μg/ml for another 45 min, leading to a decrease of urine osmolarity from 446 to 340 mosM. The body temperature was kept at 37 °C. Animals were sacrificed during narcosis by air injection into the jugular vein, and the kidneys were removed for the preparation of Western blots and immunohistochemistry. All animal procedures were performed according to national law.

Statistics

Data are expressed as arithmetic means ± S.E. Statistical analysis was made by the paired or unpaired *t* test, where applicable. Statistically significant differences were assumed at $p < 0.05$.

RESULTS

Cellular Localization of the ICln Protein in the Kidney—IGSS of ICln was used to investigate its distribution in sections of rat kidney cortex, outer medulla, inner medulla, and the inner medulla-papilla border (Fig. 2). In the cortex and the outer medulla, ICln is apparently localized mainly to the apical membrane of proximal tubular cells, whereas the cytosol and the basolateral membranes exhibit only weak signals. Similarly, only weak signals can be detected in the glomerula. In contrast, in tubules of the inner medulla and the inner medulla-papilla region, ICln can be found in the cytosol with no preferential sorting to either the apical or the basolateral side in the majority of the cells. The *lower panels* of Fig. 2 show ICln-IGSS of the inner medulla-papilla border of the kidney of a furosemide-treated rat (*lower right panel*) as compared with an untreated rat (*lower left panel*). ICln in the furosemide-treated kidney is preferentially sorted to the apical and basolateral cell membranes, whereas the signal in the cytosol is weak. The same pattern of ICln distribution can also be seen in immunoblots prepared from tissue lysates from the same region. The *inset* in the *lower right panel* shows that the fraction of membrane-associated immunoreactive ICln is increased in kidney preparations of furosemide-treated rats as compared with untreated rats.

Western Blot Analysis of Intracellular ICln Distribution in Cultured Cells

Isotonic Conditions—In NIH 3T3 fibroblasts, LLC-PK_1 cells, and MDCK cells, the bulk of the immunoreactive ICln protein is localized in the cytosol. A minor fraction can be identified in preparations of the cell membrane. The relative amount of cytosolic ICln is 92.8 ± 1.1% ($n = 26$), 62.6 ± 6.4% ($n = 18$), and 71.2 ± 12.8% ($n = 5$) in NIH 3T3 fibroblasts, LLC-PK_1 cells and MDCK cells, respectively. Accordingly, the corresponding membrane fractions amount to 7.2 ± 1.1% ($n = 26$), 37.4 ± 6.4% ($n = 18$), and 28.8 ± 12.8% ($n = 5$), respectively.

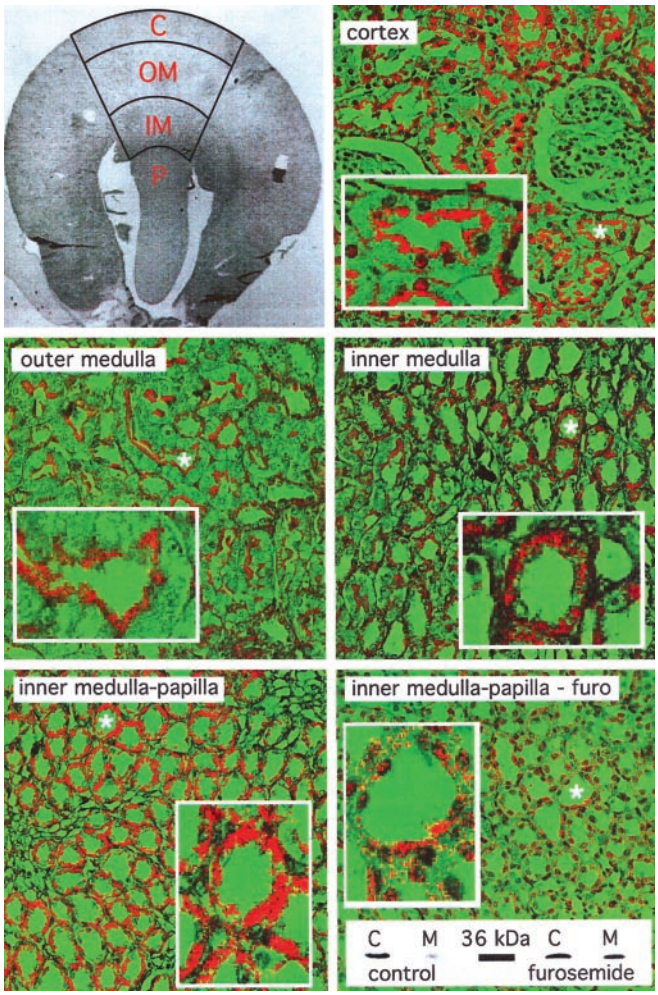

FIG. 2. **Immunohistochemical localization of ICln in the rat kidney by immunogold silver staining (IGSS, *red labels*).** IGSS were made from semi-thin sections of cortex (*C*, *top row*, *right*), outer medulla (*OM*, *middle row*, *left*), inner medulla (*IM*, *middle row*, *right*), and the inner medulla-papilla (*P*) region (*lower row*). The *upper left image* shows a cross-section of a rat kidney indicating the regions from where preparations were taken (magnification, ×10). In the cortex and the outer medulla (mainly proximal convoluted tubules and proximal straight tubules) ICln is predominantly sorted to the apical and to a lesser extent to the basolateral membrane, whereas the cytosol shows only weak signals. In the inner medulla (mainly thin limbs of Henle's loop and inner medullary collecting tubules) ICln seems to reside in the cytosol, and no clear assignment to either apical or basolateral membranes can be made. In the inner medulla-papilla border region (mainly collecting ducts) ICln is primarily located in the cytosol (*bottom row*, *left*). After furosemide treatment (*bottom row*, *right*) in most of the collecting ducts ICln is sorted predominantly to the apical and basolateral membranes. *Inset*: Western blot of cytosolic fractions (*C*) and membrane fractions (*M*) of cells from the inner medulla-papilla border region of an untreated (control, *left*) and a furosemide-treated (*right*) rat kidney. The tissues were obtained from the same kidneys used for the shown IGSS. In agreement with the IGSS images, the membrane fraction is increased after furosemide treatment. Magnification for all IGSS images is ×600. *Insets* show an enlarged view of the tubules marked by an *asterisk*.

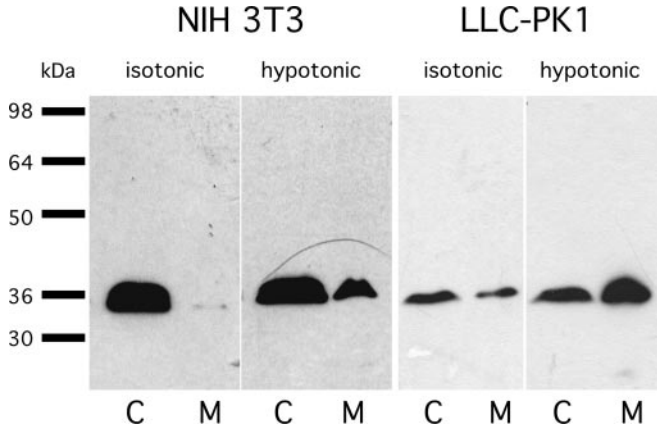

FIG. 3. **Distribution of ICln in NIH 3T3 fibroblasts (*left*) and LLC-PK$_1$ cells (*right*) (Western blots using anti-ICln antibody specifically recognizing the ICln protein at 36 kDa).** Under isotonic conditions the bulk of ICln is located in the cytoplasm. Within 15 min of hypotonic treatment the membrane fraction of ICln increases in both cell types. *C*, cytoplasmic fraction; *M*, membrane fraction.

Effect of Cell Swelling—Incubation of NIH 3T3 fibroblasts or LLC-PK$_1$ cells in hypotonic buffer for 15 min leads to a significant increase in the fraction of membrane-bound ICln protein, which is paralleled by a decrease of the cytosolic portion, indicating a cell swelling-induced shift of the ICln protein from the cytosol to the cell membrane (Fig. 3). The relative amount of cytosolic ICln decreased from 92.8 ± 1.1% to 81.0 ± 2.0% (n = 26) and from 69.8 ± 7.0% (n = 6) to 50.2 ± 12.3% (n = 6) in NIH 3T3 fibroblasts and LLC-PK$_1$ cells, respectively. Accordingly, the relative amount of membrane-bound ICln increased from 7.2 ± 1.1% to 19.0 ± 2.0% (n = 25) and from 30.2 ± 7.0% (n = 6) to 49.8 ± 12.3% (n = 6), respectively. In some preparations of both cell lines we noticed a variable increase of the total amount of immunoreactive protein.

Fluorescence Resonance Energy Transfer Measurements—Fig. 4 shows images for CFP-ICln, YFP-Mem, and NFRET under isotonic conditions and 20 min after cell swelling. CFP-ICln is distributed throughout the cytosol (*left panels*) and clear FRET signals can be detected (*right panels*), indicating an energy transfer from the CFP-ICln donors to the YFP-Mem acceptors under isotonic conditions. After cell swelling, the FRET signals are brighter and thus prove transposition of CFP-ICln protein to the cell membrane. Fig. 5*A* shows the results of the relative changes of the NFRET fluorescence intensities (ΔNFRET) 10 and 20 min after the onset of cell swelling. Using CFP-ICln as a donor and YFP-Mem as an acceptor, no significant increase in NFRET can be detected 10 min after the onset of cell swelling (18 ± 13%, n = 17), whereas after 20 min a significant increase can be observed (65 ± 23%, n = 17). Using CFP-Mem as a donor and YFP-ICln as an acceptor, a significant increase in NFRET can be detected after 10 min (18 ± 7%, n = 14), whereas after 20 min this value has decreased again (12 ± 6%, n = 14, n.s.).

To test for the differences in the subcellular localization of the swelling-induced ICln shift, ΔNFRET was calculated in 10 regions of interest (ROIs) near the outer perimeter of each cell. The results are shown in Fig. 5*B*. As evident, in most of the ROIs there is a slight decrease of NFRET after 10 min of swelling. However, in several ROIs there is a strong increase at the same time point ("hot spots"). After 20 min, most of the membrane regions exhibit a slight increase in NFRET, and the number of "hot spots" is further increased.

Measurements of Cellular Anion Entry—Time-dependent quenching of MEQ fluorescence by SCN^- entry into the cell (quenching rate; QR) was used as a measure of cellular anion permeability (Fig. 6). The QR is 0.67 ± 0.17%/s (n = 59) under isotonic conditions. Cell swelling significantly accelerates the QR to 1.11 ± 0.23%/s (n = 26). Incubation of the cells with 170 μg/ml purified ICln protein for 120 min similarly results in an increase of the QR under isotonic conditions to 1.35 ± 0.16%/s (n = 57). In ICln-CAAX-expressing cells the initial QR under isotonic conditions is identical to control cells (0.54 ± 0.15%/s, n = 27). Upon cell swelling, however, the QR is accelerated in ICln-CAAX cells (2.17 ± 0.21%/s, n = 16). Cells transfected with a control plasmid coding for a short peptide bearing the

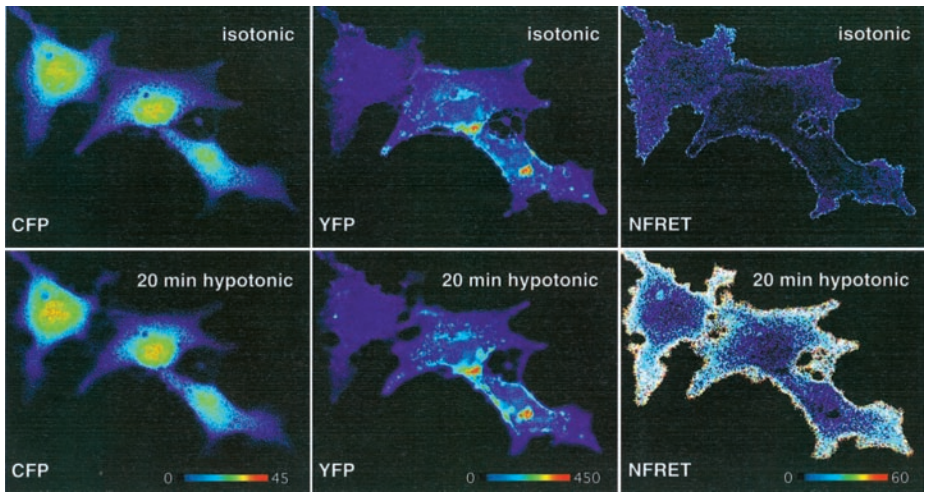

FIG. 4. **CFP-ICln and YFP-Mem FRET imaging acquired in living NIH 3T3 fibroblasts.** Cells were cotransfected with CFP-ICln (ECFP fused to the N terminus of ICln) and YFP-Mem (EYFP attached to the membrane; see also Fig. 1*A*). The images are viewed in the windows for ECFP (ex 436, em 480 nm; *left panels*), EYFP (ex 515, em 560 nm; *middle panels*), and FRET (*NFRET* = FRET after full correction for cross-talk, cross-excitation, and protein expression levels as described under "Experimental Procedures"; ex 436, em 560 nm; *right panels*) under isotonic conditions (*top row*) and 20 min after establishing hypotonic conditions (*bottom row*). The focal plane was adjusted slightly above the glass coverslip. Fluorescence intensities are given as *gray values* in *pseudocolors* (*bars*).

CAAX-motif (control-CAAX) exhibited a QR of 0.92 ± 0.11%/s (n = 31) under hypotonic conditions, which is significantly lower as compared with ICln-CAAX under the same conditions, but not different from the respective value of swollen nontransfected cells.

Electrophysiological Measurements

Whole Cell Patch Clamp and Perforated Patch Clamp Measurements—Panels A and *B* of Fig. 7 display representative original tracings of the currents elicited by step pulses to +40 mV before and 100 s after the establishment of the hypotonic conditions during the first (*A*) and second swelling (*B*) in native NIH 3T3 fibroblasts (approach 1, see "Experimental Procedures"). *Panel C* shows the time course of RVDC development of the same experiment, and *panels D* and *E* display the means from a total of 13 individual experiments, expressed either as absolute values (*D*) or as values relative to the maximum current developed during an individual experiment (*E*). *Panel F* provides the current-voltage (IV) relation immediately before and 260 s after the establishment of the hypotonic challenge for both the first and second swelling. As evident, RVDC develops more rapidly in cells facing a hypotonic condition for a second time. Upon re-establishment of the control conditions, the current is significantly reduced, and remains slightly, but significantly increased above the values observed before the first swelling. The maximum current arising during cell swelling is, however, identical under both conditions (see *panel F*).

In a separate set of experiments, a slightly modified protocol as described above was executed, in which the whole cell configuration was established shortly before the second cell swelling (approach 2). These experiments confirm the results obtained by the experiments described above and again demonstrate that the amplitude of RVDC develops more rapidly during the second hypotonic challenge. The currents measured under control conditions before and after the first swelling are not significantly different from each other. In addition, these experiments reveal that there is no shift in the reversal potential due to repeated cell swelling, indicating that the selectivity of RVDC does not change (Fig. 7*G*).

The results obtained by applying the perforated patch clamp technique (approach 3) are also in agreement with those obtained by the experiments described above: the rate of current activation and the absolute value of RVDC after 100 s of cell swelling are significantly higher during the second hypotonic challenge (Fig. 7*H*).

Using approach 1, the same experiments were performed in LLC-PK1 cells (Fig. 8, *A* and *B*) and MDCK cells (Fig. 8, *C* and *D*). Both cell types respond to the first hypotonic challenge with a comparatively slow activation of RVDC. Upon re-establishment of control conditions, however, the current does not decline in these cells, but tends to increase further. However, during the second hypotonic stimulus, RVDC develops more rapidly, and the maximum current amplitude is significantly higher as compared with the first swelling (Fig. 8, *B* and *D*).

Cell Membrane Potential Measurements—Under isotonic conditions, the PD of MDCK cells is −46.2 ± 3.0 mV (n = 6). Reduction of the extracellular osmolarity (omission of 70 mM mannitol) leads to a transient hyperpolarization (by −3.2 ± 1.3 mV, n = 6) followed by a sustained depolarization (by 15.5 ± 2.3 mV, n = 6) close to the expected equilibrium potential for chloride (37). This effect is fully reversible upon the re-establishment of isotonic extracellular conditions. Five minutes after the readmission of the isotonic solution, the PD values are not significantly different from the PD values before swelling (−46.5 ± 2.8 mV, n = 6). As shown in Fig. 8 (*E* and *F*), the second swelling of the cells causes a significantly faster depolarization: within 30 s from the peak hyperpolarization, the cells depolarize at a rate of 0.26 ± 0.05 mV/s (n = 6) upon first swelling and of 0.54 ± 0.13 mV/s (n = 6) following the second swelling. Upon the withdrawal of 150 mM mannitol, cells depolarize at a rate of 0.63 ± 0.12 mV/s (n = 5) upon the first swelling and of 0.79 ± 0.11 mV/s (n = 5) following the second swelling.

DISCUSSION

The subcellular distribution of ICln in the rat kidney shown here is in agreement with the previous observations that ICln can predominantly be found in preparations of brush border membrane vesicles from pig kidney proximal tubules, whereas vesicles prepared from the basolateral membrane and endocytotic vesicles are apparently free of the protein (38). Similar results were obtained in porcine kidneys in a study performed by Tao *et al.* (39), who observed ICln in the soluble, the microsomal, and the membrane fractions and found it to be localized on the luminal surface membranes of the distal tubules, of the ascending limbs of Henle's loop, and inside proximal tubular cells. The authors have suggested that ICln functions according to a "cytosolic anchor-membrane insertion model" and that the protein plays an important role in urine dilution (39).

Kidney tubule cells have a strong requirement for cell volume regulatory mechanisms, because they have to face severe perturbations of their cell volume. Proximal tubules perform a concentrative uptake of osmotically active solutes, early distal tubules face a hypotonic intraluminal fluid, and medullary tubules are exposed to a highly hypertonic environment during antidiuresis, which is washed out rapidly during the transition

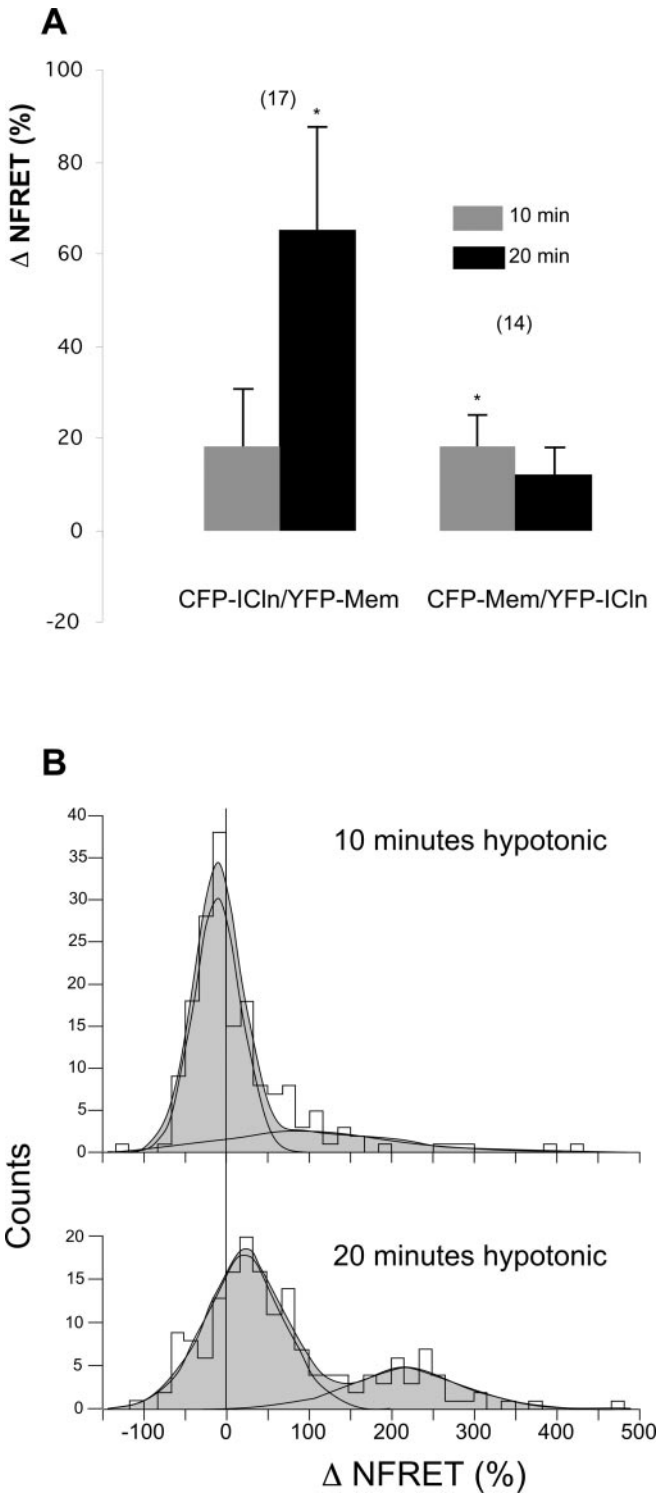

FIG. 5. *A*, relative change of CFP-ICln and YFP-Mem NFRET and CFP-Mem and YFP-ICln NFRET (ΔNFRET in %) in NIH 3T3 fibroblasts 10 min (*gray bars*) and 20 min (*black bars*) after establishment of hypotonicity. The FRET signals were collected from the images of whole-cells and are given relative to the values measured under isotonic conditions (means ± S.E.). *B*, frequency distribution histogram of the relative changes of CFP-ICln − YFP-Mem NFRET (ΔNFRET in %) 10 min (*upper panel*) and 20 min (*lower panel*) after the establishment of hypotonicity. The results were obtained from the same cells as analyzed in *panel A*, and the FRET signals were collected from ten regions of interest (ROI) located near the outer perimeter of each cell.

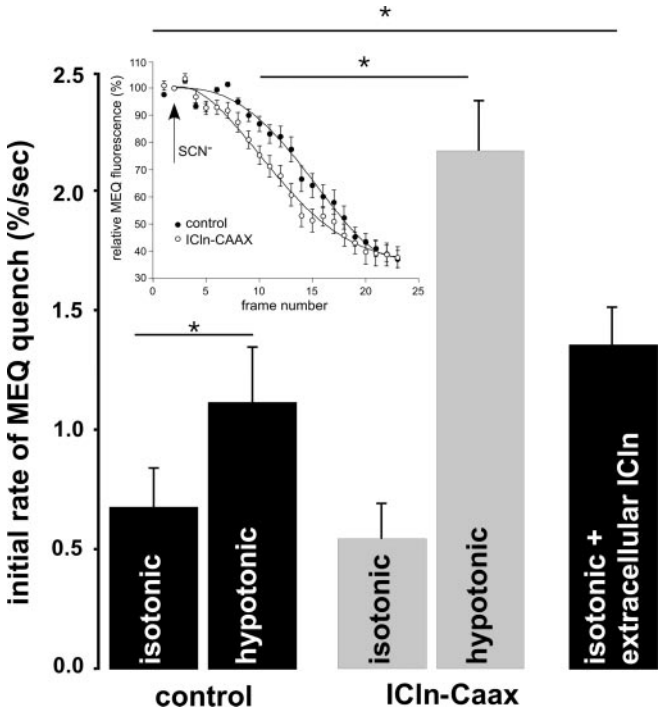

FIG. 6. **Determination of the anion permeability of NIH 3T3 fibroblasts by SCN^- quenching of MEQ fluorescence.** The initial rate of MEQ quenching is significantly enhanced in swollen cells (control, *left bars*). Enhanced association of ICln with the cell membrane by an overexpression of a farnesylated ICln protein causes a significantly faster initial quenching after cell swelling but does not increase the quenching rate under isotonic conditions (ICln-CAAX, *middle bars*). Addition of purified ICln protein to the extracellular solution enhances the quenching rate under isotonic conditions similar to cell swelling (*right bar*). *Inset*: decrease of relative MEQ fluorescence after the addition of SCN^- to the extracellular superfusate in control cells (*closed symbols*) and in the cells overexpressing ICln-CAAX (*open symbols*) (means ± S.E.).

to a diuretic state. Each of these mechanisms may lead to severe cell swelling if not properly counteracted.

To test whether the transition to diuresis affects ICln distribution in the inner medulla and papilla, rats were infused with the loop diuretic furosemide, which led to a decrease of urine osmolarity. Interestingly, ICln is preferentially sorted to the apical and basolateral cell membranes under these conditions, pointing to the possibility of a transposition of the protein, which is dependent on the functional state of the cell.

Therefore, we tested for the changes in ICln distribution in response to hypotonic cell swelling in cultured cells. In NIH 3T3 fibroblasts, LLC-PK_1 proximal tubular cells and MDCK cells, immunoreactive ICln is primarily localized in the cytosol, but a small fraction is also present in the cell membrane preparations. As shown here for NIH 3T3 fibroblasts and LLC-PK_1 cells, hypotonic treatment leads to a substantial increase in the ratio of membrane-associated ICln:cytosolic ICln (Fig. 3). Similar results were reported for rat neonatal cardiac myocytes in which ICln transiently translocates to the cell membrane, a reversible process that is paralleled by a hypotonicity-stimulated taurine efflux (40, 41). In C6 glioma cells, ~90% of ICln was found to be located in the cytosol. However, in this study, cell swelling had no effect on the relative amount of protein present in the plasma membrane fraction and transfection of these cells with a green fluorescent protein-labeled ICln construct failed to reveal any apparent membrane localization of the protein (42). Similarly, hypotonic treatment did not induce the translocation of ICln in non-pigmented ciliary epithelial cells (43).

The apparent lack of swelling-induced translocation of ICln in some cell types could be due to cell type-specific differences and/or different experimental conditions. In addition, ICln

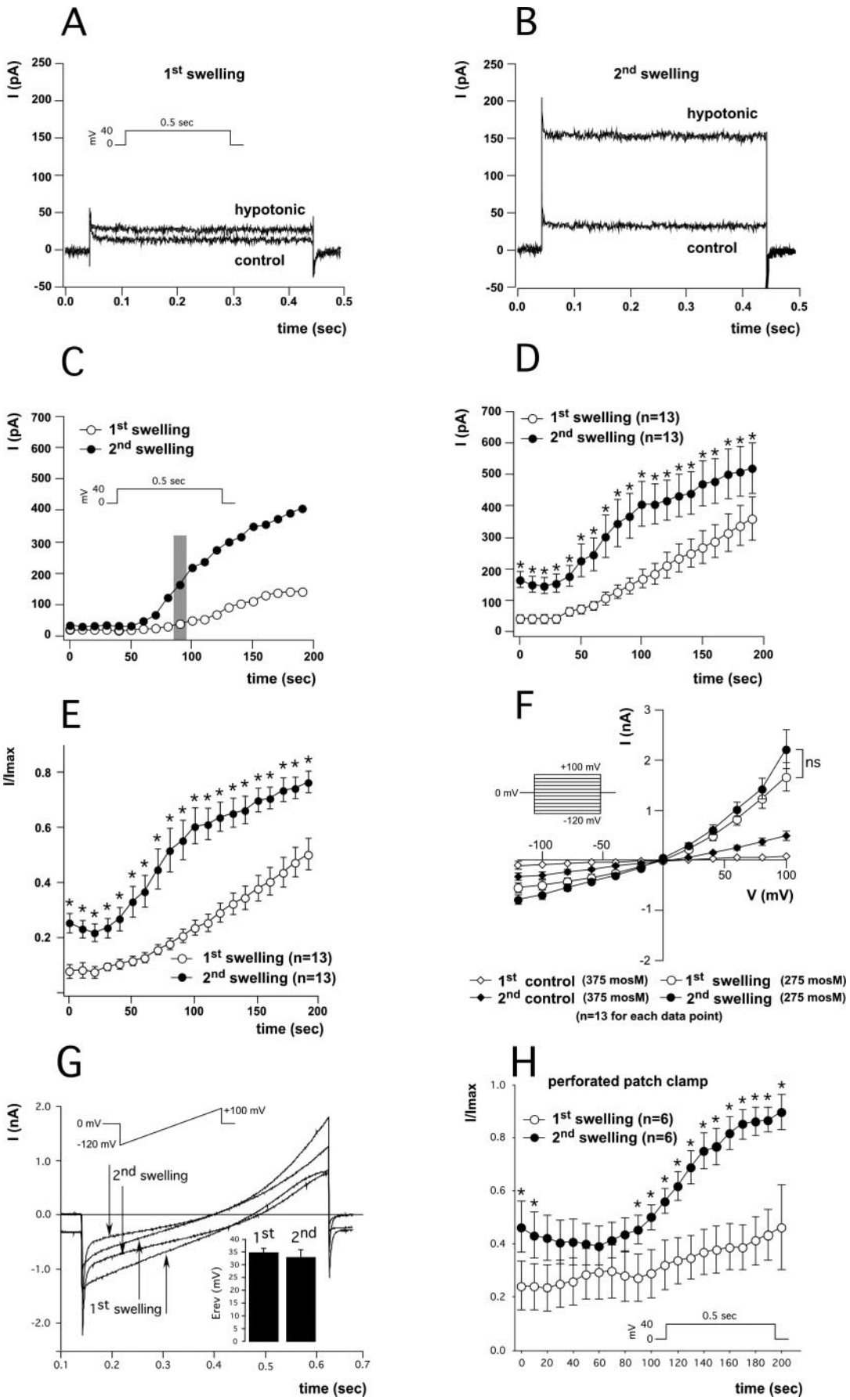

FIG. 7. **Effect of two successive hypotonic stimuli on the electrical properties of NIH 3T3 fibroblasts.** The current elicited by cell swelling (RVDC) was measured as a chloride current. *A* and *B*, representative original tracings of the currents elicited by step pulses to +40 mV before (control) and 100 s after the establishment of the hypotonic conditions (hypotonic) during the first (*A*) and second swelling (*B*). *C*, time course

translocation seems to be a transient and reversible process. Furthermore, ICln may be lost from the membrane fractions during preparation procedures.

To circumvent these problems we analyzed the transposition of ICln in living fibroblasts by fluorescence resonance energy transfer (FRET) experiments. In agreement with the results obtained from immunoblotting, fluorescently labeled ICln (CFP-ICln or YFP-ICln) is predominantly localized in the cytosol. Importantly, under isotonic conditions, clear FRET signals from the donor CFP-ICln to the acceptor YFP-Mem can be observed, unmasking a close association of the ICln protein with the cell membrane (Figs. 1 and 4). Following cell swelling, FRET signals become brighter and thus prove transposition of CFP-ICln protein to the cell membrane (Fig. 4). This transposition follows a distinct time course with detectable changes under the given experimental conditions after 20 min of hypotonicity (Fig. 5*A*). However, by swapping the donor-acceptor configuration (donor CFP-Mem and acceptor YFP-ICln) a significant increase in FRET could be detected only after 10 min of cell swelling.

The variability in the time course of the ICln transposition could be due to differences in the subcellular localization of the ICln shift. Analysis of the swelling-induced relative change of NFRET in regions of interest (ROI) at the outer perimeter of each cell (Fig. 5*B*) indeed revealed that in most of the ROIs NFRET decreases within 10 min after cell swelling. However, the simultaneous occurrence of "hot spots" discloses subcellular regions of a strong increase in FRET. After 20 min of hypotonicity, not only do the majority of the selected regions exhibit a slight increase in NFRET but also the number of "hot spots" increases further. These results clearly demonstrate that the transposition of ICln is a time-dependent process that does not occur homogenously within the membrane. Obviously there is a redistribution of ICln to regions of preferred membrane association. From the present experiments, it cannot be concluded as to whether this redistribution results from an enhanced ICln incorporation into the cell membrane or from its association with integral membrane "docking" proteins or other membrane-associated molecules.

The cellular redistribution of ICln is expected to alter some functional properties of the cell, because ICln plays an important role for RVDC. It can be expected that this process specifically modifies the ion conductance and the electrical properties of the cells. To test whether an increased presence of ICln in the cell membrane affects the cellular anion conductance, we took advantage of the fact that reconstituted ICln can directly transpose from the aqueous milieu into the membrane (14) and added purified ICln protein to the extracellular side of NIH 3T3 fibroblasts. Measurements of cellular anion entry were then performed by SCN^--quenching of the halide-sensitive fluorescent dye MEQ. In an earlier study it was demonstrated that the MEQ quench measured in NIH 3T3 fibroblasts is strongly enhanced in cells swollen by hypotonicity and that antisense oligodeoxynucleotides specifically knocking down ICln considerably impede both the MEQ quench and RVDC in NIH 3T3 fibroblasts (36). As shown in Fig. 6, incubation of NIH 3T3 fibroblasts with purified ICln protein enhances the MEQ quenching rate under isotonic conditions to a value comparable to the rate of hypotonicity-stimulated cells. To test whether an enhanced incorporation of ICln in the cell membrane from the intracellular side also results in an enhanced MEQ quenching, ICln was specifically targeted to the cell membrane by the overexpression of a farnesylated form of the protein (24, 25). In these cells the MEQ quench under isotonic conditions is identical in control cells and in ICln-CAAX cells. In the latter it is, however, strongly enhanced upon cell swelling. These experiments clearly indicate that an enhanced presence of membrane-associated ICln is accompanied by an increased anion flux. This is in agreement with previous findings showing that an enhanced ICln expression increases RVDC (11). In contrast to externally applied ICln, which *per se* leads to an enhanced anion conductance, ICln forced into or close to the cell membrane by a farnesyl anchor from the intracellular side is obviously subject to regulation by cell swelling. Li *et al.* (17) have shown that ICln, when added to the external medium bathing the Sf9 insect cells and inserted into the plasma membrane, increased the cellular cation permeability. The apparent opposite effect on the ion permeability of ICln added to the extracellular side of Sf9 cells can be explained by the unselective properties of reconstituted ICln, which has been shown to be permeable for both anions and cations (14, 16). In addition, MEQ is not sensitive to cations and therefore our experiments do not exclude a possible parallel cation entry into the cells. However, besides from being explained by an anion-conducting pathway formed by the ICln proteins themselves, the enhanced anion conductance could also arise from the activation of preexisting anion channels in the plasma membrane.

It has been demonstrated that the overexpression of ICln in human *tsA201a*, colonic (*T84*) and myeloma (RPMI 8826) cell lines accelerates the activation of RVDC after hypotonic stimulation (11) and that ICln-specific monoclonal antibodies block the activation of a native hypotonicity-induced chloride conductance in *Xenopus* oocytes (8). Because transposition of ICln protein to the membrane triggered by cell swelling could modify the electrical properties of the cells, we investigated the activation and development of RVDC, and the changes of the cell membrane potential (PD) after two successive pulses of hypotonicity in NIH 3T3 fibroblasts, LLC-PK_1 cells, and MDCK cells, respectively. As shown in Figs. 7 and 8 RVDC develops more rapidly if these cells face the hypotonic condition for a second time. Moreover, in LLC-PK_1 cells and MDCK cells, the current amplitude developing during the second period of cell swelling is higher as compared with the first swelling. Possible explanations include that channels already residing in the membrane are slowly activated by the volume stimulus and/or that more channel units are incorporated into the cell membrane. Interestingly, LLC-PK_1 and MDCK cells apparently lack an immediate recovery of RVDC following the re-establishment of control conditions. Obviously the process of RVDC activation, once initiated, prevails for at least a few minutes in these cells.

If this activation results from a swelling-induced incorporation of channel proteins into the membrane, then cells that have previously experienced swelling are expected to respond more accurately to a second hypo-osmotic stimulus due to a greater number of functional channels present in the cell mem-

of RVDC development of the same experiment. *D* and *E*, means from a total of 13 individual experiments. Currents are expressed as absolute values (*D*) or as relative values (I_{max} = maximum current developed during an individual experiment) (*E*). *F*, current-voltage (IV) relation immediately before (control, *diamonds*) and 240 s after (*circles*) establishment of the hypotonic condition for both the first (*open symbols*) and second swelling (*closed symbols*). *G*, original tracing of RVDC during a voltage ramp from −120 mV to +100 mV 3 min after the first and second swelling, respectively. The current was first measured under symmetrical conditions, and then the extracellular solution was changed to allow for the measurement of the reversal potentials. *Inset*, the reversal potentials are close to the calculated equilibrium potentials for chloride and are not significantly different after the first and second swelling. *H*, time course of RVDC development during the first and second swelling using the perforated patch clamp technique (means ± S.E.).

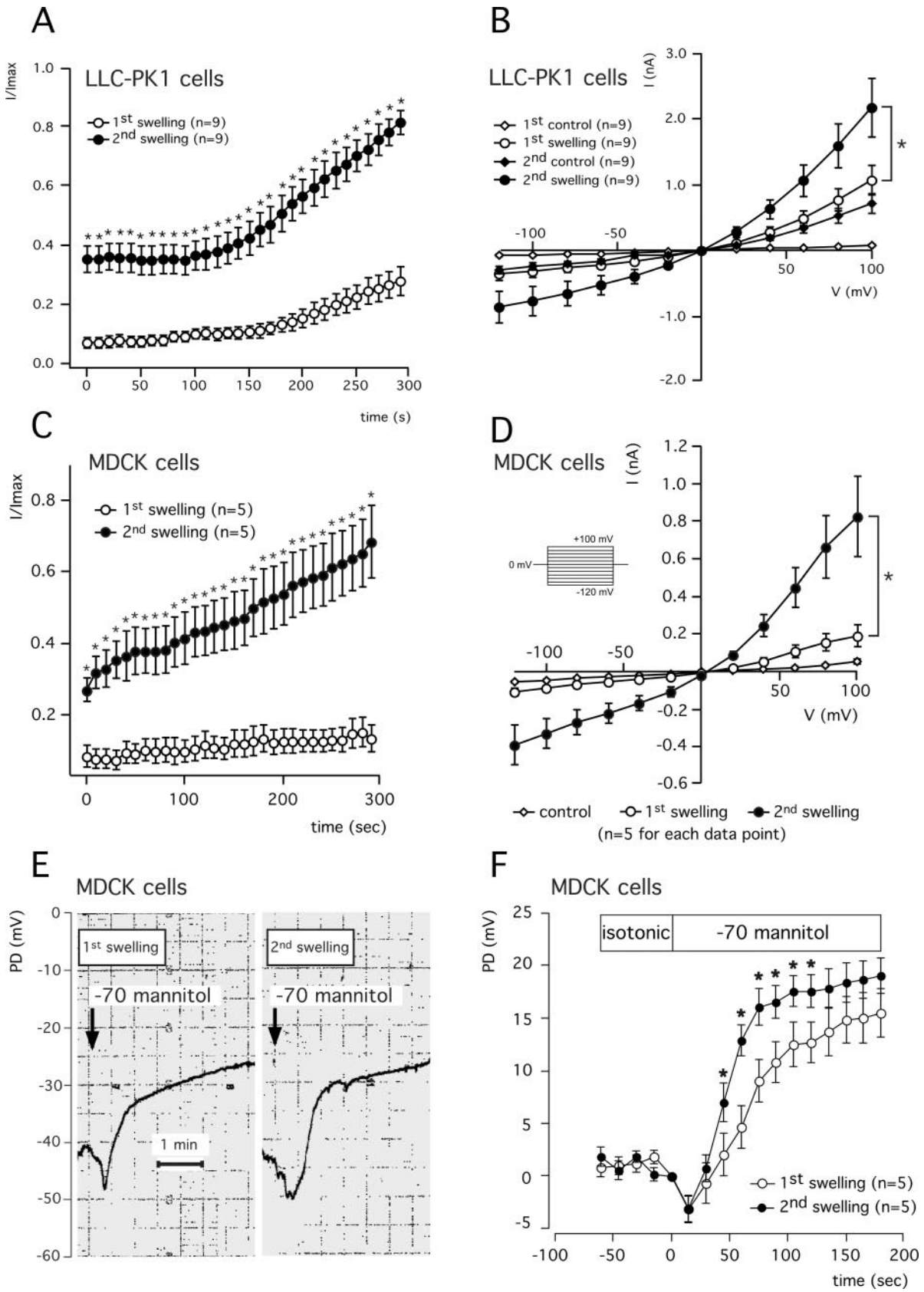

FIG. 8. *A–D*, RVDC in LLC-PK$_1$ cells (*A* and *B*) and MDCK cells (*C* and *D*) during the first (*open symbols*) and second cell swelling (*closed symbols*). *A* and *C*, time-dependent development of the currents during the first swelling (*open symbols*) and second swelling (*closed symbols*). *B* and *D*, current-voltage (IV) relation immediately before (control; *diamonds*) and 360 s after (*circles*) the establishment of hypotonicity for both the first swelling (*open symbols*) and second swelling (*closed symbols*). *E* and *F*, measurements of the cell membrane potential (PD in millivolts) of MDCK cells subjected to two successive hypotonic challenges by the omission of 70 mM mannitol from the superfusate. Each hypotonic stimulus lasted 4–5 min and was separated by a period of 5 min during which cells were superfused with isotonic solution. *E*, original tracing of a representative measurement from a single MDCK cell. *F*, time course of the swelling-induced PD changes in MDCK cells during the first (*open symbols*) and second (*closed symbols*) swelling ($n = 5$). Hypotonicity was induced by the omission of 70 mM mannitol (means ± S.E.).

brane. To test this hypothesis, MDCK cells were exposed to two successive pulses of hypotonicity, and the changes of the cell membrane potential were monitored. In previous studies we have demonstrated that MDCK cells and NIH 3T3 fibroblasts respond to cell swelling with a transient hyperpolarization (due to the activation of calcium-sensitive K^+ channels), followed by a sustained depolarization caused by the activation of an anion selective RVDC (31, 44). As shown in Fig. 8 (*E* and *F*), the cell swelling-induced depolarization is indeed significantly faster during the second swelling event as compared with the first one. In addition, it is evident that the rate of depolarization is dependent on the osmotic gradient imposed, *i.e.* cells depolarize faster if they are swollen by a stronger osmotic stimulus.

These results indicate that during cell swelling the number of functional channels in the cell membrane increases with time. After terminating cell swelling by the re-establishment of control conditions, the channels stay in the cell membrane and retain their functional state for awhile. During this time, RVDCs remain activated or can be rapidly re-activated. Such a mechanism enables the cells to accurately respond to fluctuating changes in the ambient osmolarity. The facilitation of the ability of the cells to rapidly tune their volume can be regarded as an important physiological mechanism. Whereas the immediate activation of RVDC provides a mechanism for acute volume regulation, the transposition of ICln from the abundant cytosolic pool to the cell membrane could serve as an intermediate regulation or adaptation to situations where the extracellular or intracellular osmolarities frequently change. Long term adaptation possibly involves regulation of ICln on either the transcriptional or post-transcriptional level (43, 45).

The experiments performed to verify the transposition of ICln to the cell membrane and the possible functional consequences of the enhanced protein presence in or at the cell membrane elucidated in this study do not provide insight into the mechanism of the translocation of the protein. Functional reconstitution of ICln in lipid bilayers revealed that the protein spontaneously inserts into the membrane without the need of prior incorporation into liposomes (14, 15). This demonstrates that ICln can act as an ion channel *per se* and that ICln does not necessarily need a receptor for insertion, thus suggesting a mechanism for ion channel insertion in eukaryotes, which is well established in prokaryotes (46). In some experiments we noticed an increase in the total amount of immunoreactive ICln (Fig. 3), pointing to the possibility that the process of translocation could not only be facilitated by hypotonicity itself but also be driven by a hypotonicity-induced increase in the overall levels of ICln due to enhanced synthesis or suppressed degradation of the protein. However, in human non-pigmented ciliary epithelial cells and in cultured bovine lens epithelial cells, continued hypotonic treatment did not change the expression of ICln at the protein level but did down-regulate ICln mRNA (43, 45). Regulatory factors such as intracellular calcium or pH might also play an important role for the membrane association of ICln. It has been shown that calcium, pH (14), phosphorylation (17), and lipid composition (16) can modulate the biophysical characteristics of reconstituted ICln. Besides these regulatory factors, interactions of ICln with other proteins and/or lipids promoting membrane incorporation seem most likely. Interactions of ICln have been demonstrated for cytoskeletal proteins such as actin (8, 47, 48), erythrocyte protein 4.1 (49), a human homologue of yeast Skb1 (50), and the nonmuscle isoform of the myosin light chain (51). Furthermore, ICln associates with a casein kinase I/II-like kinase (52) and the Sm proteins (20–22, 53), which are linked to the splicing machinery. Recently we have shown a functional interaction for the ICln isoform of the nematode *Caenorhabditis elegans* with a partner protein transcribed along with ICln from the operon housing these genes (15). All of these findings imply that ICln has multiple functions within the cell. Structural evidence for multiple functions of a chloride channel comes from the recent finding that CLIC1/NCC27, a member of the chloride intracellular channel (CLIC) family that is similarly able to insert directly from the cytosol into the membrane, has been identified to belong to the glutathione *S*-transferase superfamily (54). The concept of protein-multifunctionality would also help explain the lethal effect of an ICln knockout (6).

In conclusion we have shown that the multifunctional protein ICln exhibits a distinct pattern of cellular distribution in kidney tubules, depending on their parenchymal localization and functional state. In cultured cells, swelling leads to a time-dependent cellular redistribution of the ICln protein to regions of preferred association with the cell membrane. The enhanced presence of membrane-associated ICln correlates with increased anion permeability and could therefore contribute to the altered kinetics of RVDC observed in these cells after repeated cell swelling.

Acknowledgments—We gratefully acknowledge helpful discussion with Profs. R. Kinne, F. Lang, and G. Grübl and the technical assistance of A. Baumgartner. The PcDna3YFPCaaX vector was a kind gift from Dr. Kees Jalink, at the Netherlands Cancer Institute, Amsterdam.

REFERENCES

1. Lang, F., Busch, G. L., Ritter, M., Völkl, H., Waldegger, S., Gulbins, E., and Häussinger, D. (1998) *Physiol. Rev.* **78,** 247–306
2. Ritter, M., Fürst, J., Wöll, E., Chwatal, S., Gschwentner, M., Lang, F., Deetjen, P., and Paulmichl, M. (2001) *Cell. Physiol. Biochem.* **11,** 1–18
3. Fürst, J., Gschwentner, M., Ritter, M., Botta, G., Jakab, M., Mayer, M., Garavaglia, L., Bazzini, C., Rodighiero, S., Meyer, G., Eichmüller, S., Wöll, E., and Paulmichl, M. (2002) *Pfluegers Arch. Eur. J. Physiol.* **444,** 1–25
4. Jakab, M., Fürst, J., Gschwentner, M., Botta, G., Garavaglia, M. L., Bazzini, C., Rodighiero, S., Meyer, G., Eichmüller, S., Wöll, E., Chwatal, S., Ritter, M., and Paulmichl, M. (2002) *Cell. Physiol. Biochem.* **12,** 235–258
5. Scandella, E., Nagl, U. O., Oehl, B., Bergmann, F., Gschwentner, M., Fürst, J., Schmarda, A., Ritter, M., Waldegger, S., Lang, F., Deetjen, P., and Paulmichl, M. (2000) *J. Biol. Chem.* **275,** 15613–15620
6. Pu, W. T., Wickman, K., and Clapham, D. E. (2000) *J. Biol. Chem.* **275,** 12363–12366
7. Paulmichl, M., Li, Y., Wickman, K., Ackerman, M., Peralta, E., and Clapham, D. (1992) *Nature* **356,** 238–241
8. Krapivinsky, G. B., Ackerman, M. J., Gordon, E. A., Krapivinsky, L. D., and Clapham, D. E. (1994) *Cell* **76,** 439–448
9. Chen, L., Wang, L., and Jacob, T. J. (1999) *Am. J. Physiol.* **276,** C182–C192
10. Gschwentner, M., Nagl, U. O., Wöll, E., Schmarda, A., Ritter, M., and Paulmichl, M. (1995) *Pfluegers Arch. Eur. J. Physiol.* **430,** 464–470
11. Hubert, M. D., Levitan, I., Hoffman, M. M., Zraggen, M., Hofreiter, M. E., and Garber, S. S. (2000) *Biochim. Biophys. Acta* **1466,** 105–114
12. Tao, G.-Z., Kobayashi, A., Itoh, H., and Tashima, Y. (1998) *FEBS Lett.* **434,** 28–32
13. Tao, G. Z., and Tashima, Y. (2000) *Peptides* **21,** 485–490
14. Fürst, J., Bazzini, C., Jakab, M., Meyer, G., König, M., Gschwentner, M., Ritter, M., Schmarda, A., Botta, G., Benz, R., Deetjen, P., and Paulmichl, M. (2000) *Pfluegers Arch. Eur. J. Physiol.* **440,** 100–115
15. Fürst, J., Ritter, M., Rudzki, J., Danzl, J., Gschwentner, M., Scandella, E., Jakab, M., König, M., Oehl, B., Lang, F., Deetjen, P., and Paulmichl, M. (2002) *J. Biol. Chem.* **277,** 4435–4445
16. Garavaglia, L., Rodighiero, S., Bertocchi, C., Manfredi, R., Fürst, J., Gschwentner, M., Ritter, M., Bazzini, C., Botta, G., Jakab, M., Meyer, G., and Paulmichl, M. (2002) *Pfluegers Arch. Eur. J. Physiol.* **443,** 748–753
17. Li, C., Breton, S., Morrison, R., Cannon, C. L., Emma, F., Sanchez-Olea, R., Bear, C., and Strange, K. (1998) *J. Gen. Physiol.* **112,** 727–736
18. Fürst, J., Jakab, M., König, M., Ritter, M., Gschwentner, M., Rudzki, J., Danzl, J., Mayer, M., Burtscher, C. M., Schirmer, J., Maier, B., Nairz, M., Chwatal, S., and Paulmichl, M. (2000) *Cell. Physiol. Biochem.* **10,** 329–334
19. Pu, W. T., Krapivinsky, G. B., Krapivinsky, L., and Clapham, D. E. (1999) *Mol. Cell. Biol.* **19,** 4113–4120
20. Friesen, W. J., Paushkin, S., Wyce, A., Massenet, S., Pesiridis, G. S., Van Duyne, G., Rappsilber, J., Mann, M., and Dreyfuss, G. (2001) *Mol. Cell. Biol.* **21,** 8289–8300
21. Friesen, W. J., Wyce, A., Paushkin, S., Abel, L., Rappsilber, J., Mann, M., and Dreyfuss, G. (2002) *J. Biol. Chem.* **277,** 8243–8247
22. Meister, G., Eggert, C., Buhler, D., Brahms, H., Kambach, C., and Fischer, U. (2001) *Curr. Biol.* **11,** 1990–1994
23. Sambrook, J., Fritsch, E. F., and Maniatis, T. (1989) *Molecular Cloning: A Laboratory Manual*, 2nd Ed., Cold Spring Harbor Laboratory, Cold Spring Harbor, NY
24. Fürst, J., Haller, T., Chwatal, S., Wöll, E., Dartsch, P. C., Gschwentner, M., Dienstl, A., Zwierzina, H., Lang, F., Paulmichl, M., and Ritter, M. (2002) *Cell. Physiol. Biochem.* **12,** 19–30
25. van der Wal, J., Habets, R., Varnai, P., Balla, T., and Jalink, K. (2001) *J. Biol.*

Chem. **276,** 15337–15344
26. Gadella, T. W., Jr., van der Krogt, G. N., and Bisseling, T. (1999) *Trends Plant Sci.* **4,** 287–291
27. Heim, R., and Tsien, R. Y. (1996) *Curr. Biol.* **6,** 178–182
28. Pollok, B. A., and Heim, R. (1999) *Trends Cell Biol.* **9,** 57–60
29. Xia, Z., and Liu, Y. (2001) *Biophys. J.* **81,** 2395–2402
30. Llopis, J., McCaffery, J. M., Miyawaki, A., Farquhar, M. G., and Tsien, R. Y. (1998) *Proc. Natl. Acad. Sci. U. S. A.* **95,** 6803–6808
31. Ritter, M., Paulmichl, M., and Lang, F. (1991) *Pfluegers Arch. Eur. J. Physiol.* **418,** 35–39
32. Huang, W. M., Gibson, S. J., Facer, P., Gu, J., and Polak, J. M. (1983) *Histochemistry* **77,** 275–279
33. Stuart-Tilley, A., Sardet, C., Pouyssegur, J., Schwartz, M. A., Brown, D., and Alper, S. L. (1994) *Am. J. Physiol.* **266,** C559–C568
34. Bradford, M. (1976) *Analyt. Biochem.* **72,** 248–254
35. Laemmli, U. K. (1970) *Nature* **227,** 680–685
36. Wöll, E., Gschwentner, M., Fürst, J., Hofer, S., Buemberger, G., Jungwirth, A., Frick, J., Deetjen, P., and Paulmichl, M. (1996) *Pfluegers Arch. Eur. J. Physiol.* **432,** 486–493
37. Lang, F., Defregger, M., and Paulmichl, M. (1986) *Pfluegers Arch. Eur. J. Physiol.* **407,** 158–162
38. Laich, A., Gschwentner, M., Krick, W., Nagl, U. O., Fürst, J., Hofer, S., Susanna, A., Schmarda, A., Deetjen, P., Burckhardt, G., and Paulmichl, M. (1997) *Kidney Int.* **51,** 477–478
39. Tao, G. Z., Komatsuda, A., Miura, A. B., Kobayashi, A., Itoh, H., and Tashima, Y. (1998) *Biochem. Biophys. Res. Commun.* **247,** 668–673
40. Musch, M. W., Davis-Amaral, E. M., Vandenburgh, H. H., and Goldstein, L. (1998) *Pfluegers Arch. Eur. J. Physiol.* **436,** 415–422
41. Musch, M. W., Luer, C. A., Davis-Amaral, E. M., and Goldstein, L. (1997) *J. Exp. Zool.* **277,** 460–463
42. Emma, F., Breton, S., Morrison, R., Wright, S., and Strange, K. (1998) *Am. J. Physiol.* **274,** C1545–C1551
43. Sanchez-Torres, J., Huang, W., Civan, M. M., and Coca-Prados, M. (1999) *Curr. Eye Res.* **18,** 408–416
44. Paulmichl, M., Friedrich, F., Maly, K., and Lang, F. (1989) *Pfluegers Arch. Eur. J. Physiol.* **413,** 456–462
45. Reeves, R. E., Sanchez-Torres, J., Coca-Prados, M., and Cammarata, P. R. (1998) *Curr. Eye Res.* **17,** 861–869
46. Lakey, J. H., Gonzalez-Manas, J. M., van der Goot, F. G., and Pattus, F. (1992) *FEBS Lett.* **307,** 26–29
47. Schwartz, R. S., Rybicki, A. C., and Nagel, R. L. (1997) *Biochem. J.* **327,** 609–616
48. Li, Y.-Y., Tao, G.-Z., Nagasawa, H., Tazawa, H., Kobayashi, A., Itoh, H., and Tashima, Y. (1999) *J. Biochem.* **126,** 643–649
49. Tang, C. J., and Tang, T. K. (1998) *Blood* **92,** 1442–1447
50. Krapivinsky, G., Pu, W., Wickman, K., Krapivinsky, L., and Clapham, D. E. (1998) *J. Biol. Chem.* **273,** 10811–10814
51. Emma, F., Sanchez-Olea, R., and Strange, K. (1998) *Biochim. Biophys. Acta* **1404,** 321–328
52. Sanchez-Olea, R., Emma, F., Coghlan, M., and Strange, K. (1998) *Biochim. Biophys. Acta* **1381,** 49–60
53. Schmarda, A., Fresser, F., Gschwentner, M., Fürst, J., Ritter, M., Lang, F., Baier, G., and Paulmichl, M. (2001) *Cell. Physiol. Biochem.* **11,** 55–60
54. Cromer, B. A., Morton, C. J., Board, P. G., and Parker, M. W. (2002) *Eur. Biophys. J.* **31,** 356–364

Cell Swelling Stimulates Cytosol to Membrane Transposition of ICln

Markus Ritter, Andrea Ravasio, Martin Jakab, Sabine Chwatal, Johannes Fürst, Andreas Laich, Martin Gschwentner, Sara Signorelli, Carmen Burtscher, Sonja Eichmüller and Markus Paulmichl

J. Biol. Chem. 2003, 278:50163-50174.
doi: 10.1074/jbc.M300374200 originally published online September 11, 2003
